We are IntechOpen, the world's leading publisher of Open Access books Built by scientists, for scientists

5,900
Open access books available

145,000
International authors and editors

180M
Downloads

Our authors are among the

154
Countries delivered to

TOP 1%
most cited scientists

12.2%
Contributors from top 500 universities

CLARIVATE ANALYTICS
BOOK CITATION INDEX
INDEXED

WEB OF SCIENCE™

Selection of our books indexed in the Book Citation Index in Web of Science™ Core Collection (BKCI)

Interested in publishing with us?
Contact book.department@intechopen.com

Numbers displayed above are based on latest data collected.
For more information visit www.intechopen.com

5

Probing Metal/Organic Interfaces Using Doubly-Resonant Sum Frequency Generation Vibrational Spectroscopy

Takayuki Miyamae
Nanosystem Research Institute,
National Institute of Advanced Industrial Science and Technology (AIST),
Japan

1. Introduction

Recent advances in the performance of organic semiconductors such as organic light emitting diodes (OLEDs), organic field-effect transistors (OFETs), and organic solar cells have been dramatic. In particular for OLEDs, stability and durability have improved to levels that warrant their application in everyday life. In organic devices, the charge carriers, both electrons and holes, often have to be injected through organic/electrode interfaces. Therefore, an understanding of the interaction between metal electrode and organic molecules is quite important, because the electronic properties of metal/organic interface directly affect the performance of the OLEDs. (Tang & Slyke, 1987; Salaneck et al., 2002) But these are not well examined, especially the physical and chemical properties of buried organic/meal interfaces have been not well investigated. In order to understand the mechanisms that control the electron energetic levels of organic/metal interfaces, the determination of the energy barriers between the Fermi level of the metal and the HOMO and LUMO levels of organic materials across the interfaces has been main challenges to surface and interface studies of organic thin films. For understanding the occupied states, ultraviolet photoelectron spectroscopy (UPS) is one of the powerful techniques for studying the valence electronic structure of material. The electron injection barrier at the metal/organic interface is significantly altered by the interfacial dipole layer, by which the vacuum level at the organic layer is shifted relative to that at the metal layer. (Ishii et al., 1999) The dipole layer has been studied for organic/metal interfaces by using photoelectron spectroscopic technique. Ishii et al. proposed various origins of the dipole layer at the organic/metal interface: (1) charge transfer, (2) mirror force, (3) pushback effect due to the surface rearrangement, (4) chemical interaction, (5) interface state, and (6) permanent dipole of the adsorbate. (Ishii et al., 1999)

In contrast, the band gaps of the organic materials and the energy of LUMO are often determined by the optical absorption measurements of the "*bulk*". Because of the surface confinement effect and the interaction between organic molecules and metal, the molecular conformation and the band gap at the buried interface are expected to be different from those in the bulk. Although the optical band gap obtained from the absorption spectroscopy is different from the corresponding charge transfer gap due to the exciton absorption to

form Frenkel-type exciton, the optical band gaps at buried interfaces are still useful energy parameter to discuss the charge injection and overall efficiency of the OLED. However, it has been a great challenge to measure the buried interfacial electronic states because of a lack of a suitable probing technique. Traditional surface science techniques based on ultrahigh vacuum are not applicable to a buried interface, and absorption and emission spectroscopy do not have the necessary surface sensitivity.

Nonlinear optical spectroscopy is one of the powerful techniques for the characterization of these issues due to its high interface sensitivity. Second harmonic generation (SHG) and sum frequency generation (SFG) have been used to investigate the molecular orientation of the materials at the interface. (Shen, 1984) IR-visible SFG spectroscopy has made it possible to study the vibrational spectra of surface or interfacial species. SFG is a surface-sensitive tool because its second-order nonlinear optical process is allowed only in non-centrosymmetric media under the electric dipole approximation. Recently this technique has been applied to interfaces that include organic materials, allowing the interfacial structures to be elucidated. In our SFG studies of polymer/water, (Miyamae et al., 2007) polymer/oxide, (Miyamae & Nozoye, 2004) and air/liquid interfaces, (Miyamae et al., 2008; Iwahashi et al., 2008) we have found that the molecular structures, such as the orientation and orientation distribution of different chemical groups, are not the same at the different interfaces.

IR-visible SFG spectroscopy has been traditionally carried out by using the frequency-fixed visible and tunable IR beams to obtain a surface vibrational spectrum, which identifies the surface chemical species. Recently, a new technique for vibrational SFG spectroscopy by tuning the incident visible and IR frequencies has attracted much attention. (Raschke et al., 2002) When the photon energy of the SFG coincides with electronic transition energies of interface species, the output SFG intensity is drastically enhanced when the IR light is resonant with the vibrational state and the output SFG light is resonant with the interfacial electronic transitions. Such enhanced SFG process is called doubly-resonant (DR) SFG. With the capability of tuning both the incident IR and visible frequencies, doubly-resonant SFG spectroscopy becomes a powerful multi-dimensional technique for studying the interface electronic states coupled to a specific vibrational mode. The SFG electronic excitation profiles, which can be obtained by measuring the visible probe frequency dependence of the vibrational SFG band strengths, allow deduction of coupling electronic transitions and vibrational modes at the interface. (Miyamae et al., 2009)

In addition, there are several advantages of the doubly-resonant SFG technique. The signal enhancement is expected only for species that have an electronic absorption at the photon energy of the SFG. Therefore, doubly-resonant effect offers a kind of molecular selectivity to SFG. Moreover, an electronic excitation spectrum of the interface species for each vibrational band can be obtained. Thus the SFG excitation profiles are useful to investigate mixed interface layers where several chemical species coexist and show complex vibrational spectra, because vibrational bands can be classified with reference to corresponding electronic spectra. In addition, the measurement of SFG excitation profiles may be an effective way to obtain electronic spectra of the molecules, especially at interface on opaque substrates where electronic absorption spectrum measurement is difficult. Furthermore, it can be possible to measure the interface of the OLED materials that show very strong photoluminescence in visible region, since the output SFG emerges at the Anti-Stokes side of the excitation wavelength.

This chapter is constructed as follows: in Section 2, we describe the theoretical backgrounds of the DR-SFG processes. Section 3 describes the experimental setup for the DR-SFG measurements and the sample preparation. Section 4 illustrates the DR-SFG study of the electronic and vibrational properties of the OLED interfaces. The chemical structures of all the organic compounds involved in this chapter are sketched in Figure 1.

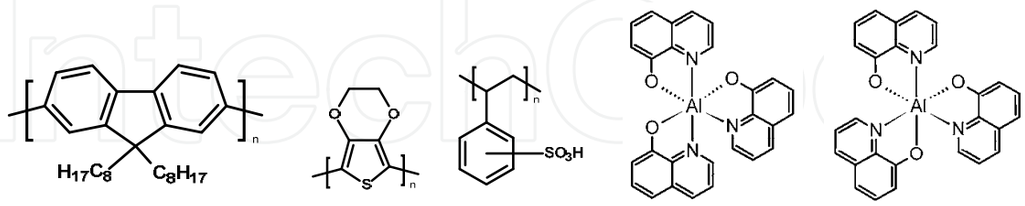

Fig. 1. Chemical structure of the various organic compounds under study: (a) PFO, poly(9,9-dioctyl-fluorene); (b) PEDOT:PSS; (c) meridional Alq_3, tris(8-hydroxyquinoline) aluminum; (d) facial Alq_3.

2. Theoretical background of the doubly-resonant sum frequency generation.

In the electric dipole approximation, SFG is forbidden in centrosymmetric materials, but not at their interfaces, where the inversion symmetry of the bulk is broken. For such an air–metal interface, the SFG intensity reflected from the surface is given by

$$I(\omega_{SF}) \propto \left| \chi^{(2)}_{eff} : E(\omega_{IR}) E(\omega_{VIS}) \right|^2 , \tag{1}$$

where $\chi^{(2)}_{eff}$ is the effective second-order nonlinear susceptibility tensor and $E(\omega_{IR})$ and $E(\omega_{VIS})$ are the input fields. The second-order nonlinear susceptibility contains nonresonant, singly resonant, and doubly resonant contributions. The latter dominates strongly if the vibrations (ω_l) and electronic transitions (ω_{eg}) probed by ω_{IR} and ω_{SFG} are coupled. Both IR–visible (vibrational transition followed by an electronic transition) and visible–IR processes (electronic transition followed by a vibrational transition) contribute to doubly–resonant SFG.(Raschke et al., 2002; Hayashi et al., 2002) However, the IR–visible sequence is expected to dominate, as a result of the quicker relaxation of the electronic excitation compared to the vibrational one. Assuming harmonic potential surfaces for the electronic states and the Born–Oppenheimer and Condon approximations, the doubly–resonant $\chi^{(2)}_{ijk}$ can be described as

$$\chi^{(2)}_{ijk} = -\frac{N}{\hbar^2} \left\langle \mu^i_{eg} \mu^j_{ge} \frac{\partial \mu^k_{gg}}{\partial q_l} \frac{\sqrt{S_l} e^{-S_l}}{\omega_{\mathrm{IR}} - \omega_l + i\Gamma_l} \times \sum_{n=0}^{\infty} \frac{S_l^n}{n!} \left\{ \frac{1}{\omega_s - n\omega_l - \omega_{eg} + i\Gamma_{en,g0}} - \frac{1}{\omega_s - (n+1)\omega_l - \omega_{eg} + i\Gamma_{en+1,g0}} \right\} \right\rangle + \chi^{(2)}_{NR,ijk} , \tag{2}$$

where N is the surface molecular density, $\mu_{eg}{}^i$ represents the i component of electronic transition moment, q_l is the normal coordinate, S_l is a dimensionless coupling constant

known as the Huang-Rhys factor, n labels the vibrational state, g and e label the ground and excited electronic states, respectively, ω_S is the SFG frequency, ω_l and ω_{eg} are the resonant vibrational and electronic frequencies, respectively, Γ_l and $\Gamma_{en,g0}$ are the damping constants, the angular brackets indicate an average over molecular orientations, and $\chi^{(2)}_{NR,ijk}$ describes the non-resonant contributions. S_l is related to the shift d_l of the harmonic potential of the vibration in the excited electronic level by

$$S_l = \frac{1}{2\hbar}\omega_l d_l^2 \quad . \tag{3}$$

As shown in Fig. 2, DR-SFG occurs thus for $\omega_{IR} = \omega_l$ and for several visible frequencies, when ω_S matches an allowed vibronic transition to the excited electronic level. The intensity of each vibronic resonance depends on the Frank-Condon overlap integrals of the vibrational levels involved in the transition. Since the initial and final vibrational states, respectively of the visible and SFG transitions, always differ, the vibration and the electronic transition must therefore be coupled ($d_l \neq 0$) to have a non-zero transition probability for the global DR-SFG process. Thus the DR-SFG spectrum allows for the determination of the coupling strength and characteristics.

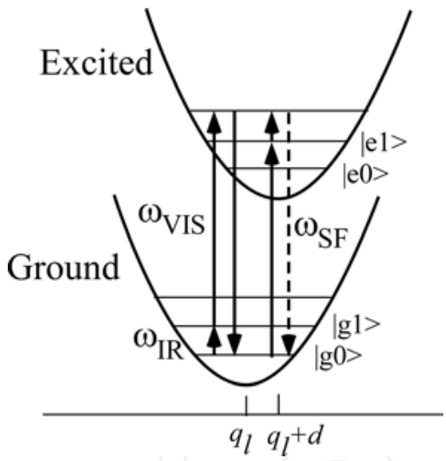

Fig. 2. Energy diagram for DR-SFG. The vibration harmonic potentials are shifted between the ground and excited states. The resonant transitions involved in the DR IR–visible (and visible–IR) sum-frequency generation processes are shown schematically.

Equation (2) includes all the vibronic transitions series. However, in general, the visible–IR SFG is much weaker and not detected because of the very fast relaxation of the electronic excitation. For example, the dephasing times of vibronic transitions are in the femtosecond region for Alq_3. Therefore, by assuming $\Gamma_{en,g0} >> \Gamma_{e0,g0}$, the nonzero vibronic transitions can be neglected.

It is worth pointing out that a significantly larger $\Gamma_{en,g0}$ also suppresses the aforementioned visible–IR SFG, which starts with an electronic transition followed by a vibrational transition.

To analyze the spectra, we note that with the visible input frequency ω_{vis} fixed, Eq. (2) can be approximated by the form

$$\chi_{ijk}^{(2)} \propto \sum_l \frac{A_l}{\omega_{\mathrm{IR}} - \omega_l + i\Gamma_l} + \chi_{NR}^{(2)} e^{i\xi} , \tag{4}$$

where A_l, ω_l, Γ_l are the peak amplitude describing the electronic resonance, the resonant vibrational frequencies, and the damping constants, respectively. $\chi^{(2)}_{NR,ijk}$ and ξ describes the non-resonant contributions and the phase difference between resonant and non-resonant term, respectively. We use Eq. (4) to fit all the measured spectra with ω_l, Γ_l, A_l, ξ, and $\chi^{(2)}_{NR}$ as adjustable parameters.

3 Experimental methods and materials

3.1 Doubly-resonant sum frequency generation

Figure 3 schematically depicts the SFG experimental setup for the doubly-resonant SFG measurements. (Miyamae et al., 2009 & 2011) Tunable IR and visible laser beams were generated by two optical parametric generators/amplifiers (OPG/OPA, Ekspla, PG401VIR/DFG) pumped by a mode-locked Nd:YAG laser at 1064 nm (Ekspla, PL-2143D, 25ps, 10Hz). The IR beam, tunable from 1000cm^{-1} to 4300 cm^{-1}, was produced by difference frequency mixing of the 1064 nm beam with the output of a LiB_3O_5 (LBO) crystal mounted in OPG/OPA, which is pumped by the 355 nm beam. The visible beam, tunable from 420 to 640 nm, was generated in a LBO crystal mounted in OPG/OPA pumped by the 355 nm beam. The visible and IR beams were overlapped at sample surface with the incidence angles of 70° and 50°, respectively. The spectral resolution of the tunable visible beam was about 8 cm^{-1}, and its frequency was calibrated with the Hg lines. The spectral resolution of the IR beam was 6 cm^{-1}, and the IR frequency was calibrated with the absorption lines of polystyrene standard. In order to minimize the irradiation damage, both tunable infrared and visible beams were defocused. The focus size of the infrared and visible beams were >1 mm and >3 mm, respectively. Further, in order to avoid photo-irradiated damage, the fluence of the visible beam was kept below 100 μJ per pulse. The absence of the damage effect was confirmed by repeated SFG measurements. In order to eliminate the scattered visible light and the photoluminescent light from the samples, the sum-frequency output signal in the reflected direction was filtered with short-wave-pass filters (Asahi Spectra Co. Ltd.), prism monochromator (PF-200, Bunkoukeiki Co., Ltd.), and grating monochromator

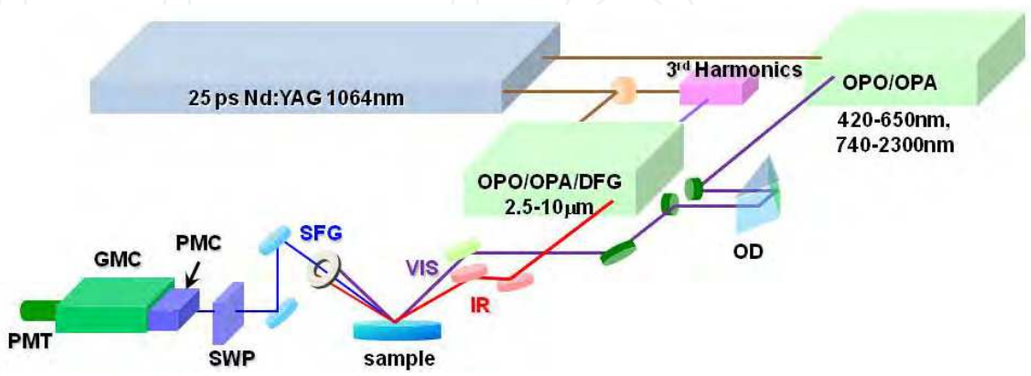

Fig. 3. The schematic arrangement of the SFG spectrometer for the DR-SFG. OD; Optical delay, SWP; short wave pass filters, PMC; prism monochromator, GMC; grating monochromator, PMT; photomultiplier tube.

(Oriel MS257). Then the SFG signal was detected by a photomultiplier tube (Hamamatsu R649). The signal was averaged over 300 pulses by a gated integrator for every data point taken at a 3 cm^{-1} interval and was stored in a personal computer. In the frequency region between 2000 and 1300 cm^{-1}, significant portion of the infrared beam is absorbed by water vapor in the optical path. The effect was minimized by purging the optical path of the IR beam and the sample stage by dry nitrogen gas. Each SFG spectrum was normalized to the visible and IR power to compensate the laser intensity fluctuations.

3.2 Sample preparations for the SFG measurements

3.2.1 Preparation of the PFO samples

The samples of the PFO endcapped with dimethylphenyl (MW=48.8K) were obtained from American Dye Source and used as received. Thin film of the PEDOT:PSS solution (CREVIOS Al4083) was spin-coated at 3000 rpm on the top of the fused quartz or CaF_2 substrates and then baked at 150 °C for 60 min in an oven with N_2 flow. PFO layer was then spin-coated at 3000 rpm from 1% w/v toluene solution on top of the PEDOT:PSS layer. Then the films were evacuated to eliminate residual solvent.

For the measurements of the buried Al/LiF/PFO interface, the LiF and the Al were directly deposited on the spin-coated PFO/PEDOT:PSS onto CaF_2 substrates in a vacuum chamber. The thicknesses of the LiF and Al are about 1 and 40 nm, respectively.

3.2.2 Preparation of the Alq_3 samples

For the preparation of the Alq_3/Al samples, the Al substrates were prepared by vacuum evaporation of Al on Si substrates by using a tungsten filament. Here, the notation of *A*/*B* indicates a system prepared by depositing *A* on *B*. Deposition of Alq_3 was performed using a quartz crucible coiled with a tungsten wire heater. Alq_3 were deposited on them under dark condition in a vacuum chamber. In order to avoid the influence of the air, 50 nm thick CaF_2 was deposited after the deposition of the 2 nm thick Alq_3. For the observation of the Al/Alq_3 interfaces by SFG, the Alq_3 films were directly deposited on CaF_2 substrates, and thick Al layers were then deposited under dark condition. For Al/LiF/Alq_3, thin LiF film of 1 nm thick was deposited on the Alq_3 from a tungsten basket. Then 50 nm thick Al layer was deposited on the LiF layer. After the deposition, the SFG measurements were subsequently performed in ambient conditions.

4. DR-SFG study of organic/metal Interfaces

4.1 DR-SFG study of poly(9,9-dioctylfluorene) surfaces and Al/LiF interfaces

Polymer LEDs are one of the most promising applications given the current high interest in developing ultra thin computer monitors and television sets, i.e., flat-panel displays. The research on polymers in LEDs has undergone a rapid expansion beginning in 1990, when results on a light-emitting diode with poly(*p*-phenylenevinylene) (PPV), as the emitting layer was published. (Burroughes et al., 1990) Recently, one particular classes of conjugated polymers, the poly(9,9-dioctylfluorene) (PFO, chemical structure is shown in Fig. 1) and fluorene-arylene copolymers have been studied intensively because of its applications in the LEDs due to their highly efficient blue photoluminescence. (Mallavia et al., 2005) Although the bulk electronic and optical properties of PFO have been studied extensively by UV-visible absorption, Raman, and photoluminescence spectroscopy,(Ariu et al., 2000; Montilla

& Mallavia, 2007) the optical and electronic properties of PFO at the buried electrode interface remain unexplored. Because the electronic properties of electrode/organic interface affect the performance of the organic LEDs, understanding of the interaction between the electrode and organic molecules and the electronic structures at the buried interfaces are quite important. In an organic device, the charge carriers have to be injected through polymer/electrode interfaces. Therefore, the band gaps of conjugated polymers at the buried interface are important energy parameters to discuss the charge injection and overall efficiency of the organic devices. In this study, we present the surface and the buried interfacial vibrational and electronic structure of the PFO using SFG. (Miyamae et al., 2010)
Figure 4 shows the SFG vibrational spectra from the PFO/PEDOT:PSS/quartz surface with various visible wavelengths in a SSP configuration (S-, S-, and P-polarized for SFG, visible, and IR, respectively). SFG susceptibility of the quartz is expected to be approximately constant in the visible region because it is transparent to visible light. A strong vibrational band was observed at 1610 cm^{-1} in all spectra, and the band intensity increased when the visible probe wavelength was changed from 550 to 435 nm. The vibrational band at 1610 cm^{-1} is assigned to the C=C symmetric stretching of the fluorene rings located at the backbone of PFO. The electronic resonance enhancement of the SFG spectra is observed when the visible wavelength is near 435 nm, which produces a SFG wavelength near 407 nm with an IR beam of 1610 cm^{-1}. It should be noted that the PFO surface does not change during the SFG measurements. It has been reported that the oxidative defect are formed during the operation or UV light irradiation. (List & Guentner, 2002; Gong et al., 2003) The UV-visible and IR absorption signature allow an identification of the defects as ketone groups attached to the 9-position of the fluorene unit; thus, the fluorene unit becomes a 9-fluorenone due to oxidative degradation. The SFG spectra clearly shows that the absence of the oxidative peak derived from the fluorenone, indicating that the PFO surface is not oxidized during the SFG measurements.

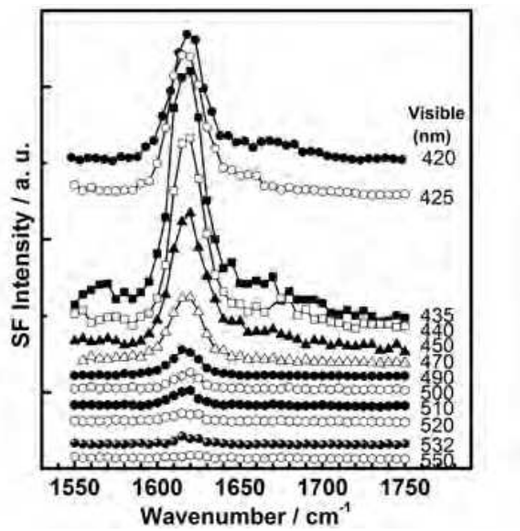

Fig. 4. SFG vibrational spectra of PFO surface with various incident visible wavelengths. Spectra are offset for clarity

Next, we show in Figure 5 the SFG spectra from the buried Al/LiF/PFO interface with various visible wavelengths in SSP polarization combination. In this project, the LiF and the Al layers were directly deposited on the spin-coated PFO/PEDOT:PSS onto CaF_2 substrate. Since the

deposited Al layer can act as superior gas barrier, the extent of the oxidation of the Al interfaces is expected to be much reduced. The vibrational band at 1610 cm^{-1} is still observed in all SFG spectra. As discussed later, the 1610 cm^{-1} peak is not derived from the buried PFO/PEDOT:PSS interface due to the less orientational order at the polymer/polymer interface. The peak position of the band does not change between the PFO surface and the PFO interface, indicating that the PFO is not degradated by the Al deposition. In the case of the DR-SFG spectra of the Al/LiF/PFO interface, it should be noted that the SFG peak shows different shape from that of the air/PFO interface. This difference is caused by the different interference phenomena with the SFG non-resonant contribution arising from the Al substrate.

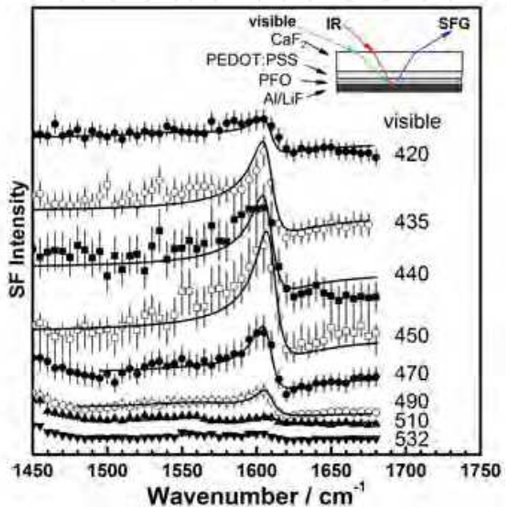

Fig. 5. The SFG spectra of buried Al/LiF/PFO interface with various incident visible wavelengths. The experimental data and the fitted curves using eq. 4 are represented by dots and solid lines, respectively. Experimental SFG setup for probing the buried interface is shown in the inset. Spectra are offset for clarity.

Because of the electronic transitin of the PFO, the refractive index of PFO in the investigated region is wavelength-dependent. (Campoy-Quiles et al., 2005) Therefore, the Fresnel factors need to be considered to obtain the actual dispersion relation of the second-order nonlinear susceptibility. In the electric-dipole approximation, the effective second-order nonlinear susceptibility tensor for the SSP polarization can be written as

$$\chi_{eff}^{(2)} = L_{YY}(\omega_{SF})L_{YY}(\omega_{VIS})L_{ZZ}(\omega_{IR})\sin\beta_{IR}\chi_{yyz}^{(2)}, \tag{5}$$

where $L_{YY}(\omega)$ and $L_{ZZ}(\omega)$ are the Fresnel coefficients at frequency ω; β_{IR} is the reflection angle of the IR frequency; and χ_{yyz} is the nonvanishing yyz component of the second-order nonlinear susceptibility in the laboratory coordinate. In the SSP polarization, the Fresnel factor can be written as

$$F_{yyz} = \left|L_{YY}(\omega_{SF})L_{YY}(\omega_{VIS})L_{ZZ}(\omega_{IR})\sin\beta_{IR}\right|, \tag{6}$$

The refractive indices for PFO and metallic aluminum reported by Campoy-Quiles et al. (Campoy-Quiles et al., 2005) and the literature (Parik, 1985) were used for the evaluation of the Fresnel factors.

In general, there are two types of processes in IR-visible SFG, as mentioned in the theoretical section. The first type starts with an electronic transition followed by a vibrational transition (VIS-IR SFG), and the second type begins with a vibrational transition followed by an electronic transition (IR-VIS SFG). (Hayashi et al., 2002) Because the electronic relaxation times are generally much shorter than the vibrational relaxation times, the contribution of the VIS-IR SFG is generally negligible. If the VIS-IR SFG occurs, increase of the non-resonant background is expected due to the ultrafast dephasing dynamics of the S_1 state. (Wu et al., 2009) Therefore, only the IR-VIS SFG will be considered in the following analysis.

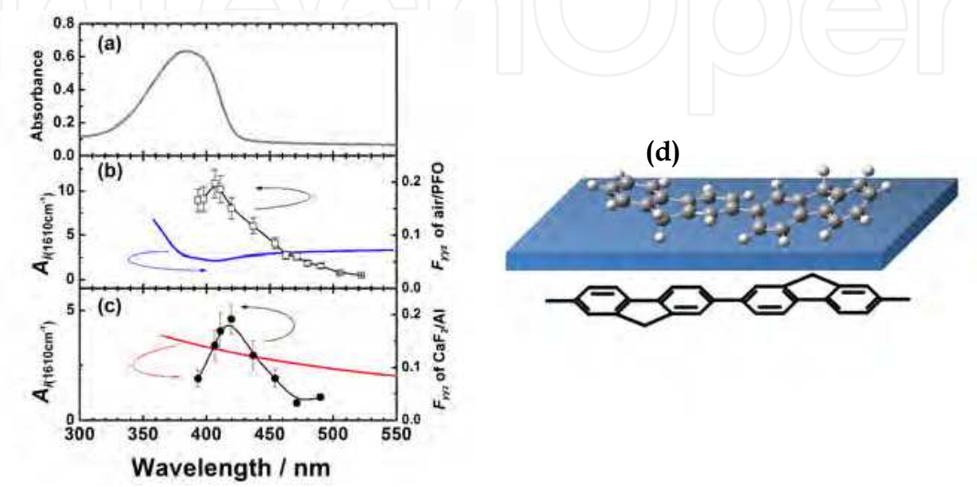

Fig. 6. (a) Optical absorption spectrum of the PFO spin cast film. (b) The SFG electronic excitation profile of air/PFO interface and the Fresnel factor F_{yyz} (continuous blue curve) at air/PFO interface, and (c) the SFG electronic excitation profile of Al/LiF/PFO interface and the F_{yyz} at CaF_2/Al interface (red curve). Solid black lines are guide to the eyes. (d) Proposed model for the planar configuration at the interface.

The curves b and c in Figure 6 show the changes in the A_l of the 1610 cm^{-1} peak deduced from the fitting of the DR-SFG spectra in Figs. 4 and 5 as a function of the photon energies of the SFG. Figure 6a shows the optical absorption spectrum of the PFO spin cast film. The broad optical absorption band originates from inhomogeneously broadened $\pi \rightarrow \pi^*$ transitions of the glassy PFO. (Cadby et al., 2000) As shown in Fig. 6, the SFG electronic excitation spectrum obtained from the air/PFO interface is slightly red-shifted with respected to an optical absorption maximum of PFO film. The SFG excitation spectrum at the Al/LiF/PFO interface is also plotted in Fig. 6c, and it is further red-shifted with respected to that of the PFO surface. It should be noted that these red-shifts are not caused by the visible variations of the Fresnel factors. As shown in Fig. 6, the wavelength variations of the F_{yyz} both air/PFO and CaF_2/Al interfaces do not explain the SFG electronic excitation profiles of the air/PFO and the buried interface. Thus we conclude that the changes of the Fresnel factors do not much affect on the spectral shape of the SFG excitation profile of the 1610 cm^{-1} peak.

We attribute that the origin of the red-shifts of the SFG electronic excitation spectra from the air/PFO and Al/LiF/PFO interfaces are due to the stress-induced surface confinement effects of the polymer backbone, as in the case of the MEH-PPV interfaces. (Li et al., 2008) In general, the optical band gap of a conjugated polymer is closely related to the conjugation length. Conjugated polymer chains consist of a series of connected segments, each of which

has a different extent of π-electron delocalization. Although the extent of the conjugation is limited by the twists in the polymer backbone, the longer the segment is, the smaller the optical band gap of the conjugated polymers due to the increasing average effective conjugation length. The restriction of the torsion angle between adjacent segments at the air/polymer and the Al/LiF/polymer interfaces produce a longer conjugation length. Similar red-shift of the electronic excitation profile at the interface has been also reported by the SFG measurements for the MEH-PPV interfaces. (Li et al., 2008)

To gain further structural information at the PFO surface, we performed the SFG measurements in the CH stretching region. The SSP SFG spectrum of the PFO surface taken at the visible wavelength of 532 nm exhibits peaks derived from the aliphatic hydrocarbon peaks that originate from the side chain of PFO, as shown in Fig. 7a. The tiny SFG signals derived from the CH stretching mode of PFO ring are observed around 3050cm^{-1} at the visible excitation wavelength of 532 nm. We also tried to measure the SPS and PPP polarization combinations, however, the intensities of the peak around 3050 cm^{-1} in SPS and PPP were much weaker than those of SSP spectra. One may think that the PFO surface must be covered with the side chain of the PFO because the peaks derived from the aliphatic hydrocarbon peaks are clearly detected. However, this 3050 cm^{-1} peak is clearly observed when the visible excitation wavelength is changed to shorter wavelength, as shown in Fig. 7. This result indicates that the planes of PFO rings are nearly parallel to the surface plane at the air/PFO interface, and the PFO surface is not fully covered with the aliphatic side chains. If the molecules take a planar orientation at the surface, it is hard to detect in SFG without the electronic resonance. It is well known that planar ordering of the polymer chains parallel to the interfaces due to the confinement effects occurs and this creates highly anisotropic optical properties to the film surface. (Kawana et al., 2002; Knaapila et al., 2003) The planar ordering of the polymer chains at the surface is in good agreement with the X-ray diffraction studies and the optical investigation by emission spectroscopy.(Cheum et al., 2009)

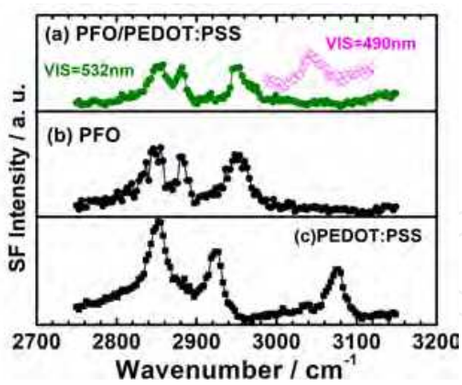

Fig. 7. SFG spectra of (a) PFO on quartz substrate taken by the 532nm (●) and 450nm (○), (b) PFO/PEDOT:PSS on quartz, and (c) PEDOT:PSS on quartz.

It is well known that the bulk solid PFO film exhibits complex phase behavior. Disordered PFO forms the glassy phase where the polymer backbones do not form a particular conformation with long-range order. In contrast, PFO in the so-called β-phase is extended conformation of PFO chains and possesses lower energy, due to the backbone planarization. (Grell et al., 1999) Single molecule spectroscopy demonstrates that the β-phase features of PFO are the results of stress-induced backbone planarization of polymer chain. (Becker &

Lupton, 2009) The optical absorption spectra of β-phase PFO exhibits the characteristic shoulder absorption around 430 nm in comparison with the glassy PFO. The SFG electronic profiles of the PFO interfaces have maximum around 410 – 420nm, and this peak position is close to the shoulder absorption of the β-phase PFO, rather than that of the glassy PFO. Because of the restriction of the torsion angle between adjacent segments, the conformation of the polymer backbone is limited at the polymer interfaces. As a result, the effective conjugation length at the interface is increased. Thus we conclude that the optical band gaps at the Al/LiF/PFO interfaces become smaller than that of the bulk glassy PFO, due to the stress-induced chain planarization at the air/PFO and the Al/LiF/PFO interfaces. The appearance of β-phase in the PFO films can be affected by many experimental treatments, such as, thermal annealing, organic solvent vapor exposure, mechanical stress, chemical modification of PFO chains, and so on. (Zhu et al., 2008) In addition to these treatments, our findings indicate that the interface confinement effect is also affected to induce the planar orientation of the polymer chains. Proposed planar orientation of the PFO chains at the interfaces is shown in Fig. 6 (d).

Figure 7 also indicates that the SFG signals are not derived from the buried PFO/PEDOT:PSS interface. To endure the observed SFG is truly generated at the air/PFO interface without a contribution from the buried PFO/PEDOT:PSS interface, we compare the SFG spectra for the PFO coated on PEDOT:PSS and the PEDOT:PSS films in the CH stretch region. The SFG spectrum of the PEDOT:PSS exhibits three vibrational resonances from CH stretches at 2855, 2927, and 3074 cm^{-1}. (Silva & Miranda, 2009) With an additional PFO layer, the SFG spectrum changes both in intensity and shapes. The SFG spectra of the PFO on PEDOT:PSS layer is very close to that of the PFO. Consequently, the topmost molecular orientation of the PEDOT:PSS does not affect the surface molecular orientation of the PFO. From this observation, we conclude that only the topmost layer has a net orientational order and contributes to the SFG spectra while the interface between PFO and PEDOT:PSS does not have contributions to the SFG spectra due to less orientational order that is inactive for SFG.

4.2 DR-SFG study of tris-(8-hydroxy-quinoline) aluminium (Alq_3)/Al interfaces

4.2.1 DR-SFG study of Alq_3 films: Peak assignments and the thickness dependences

In this section, DR-SFG was applied to detect the interfacial vibrational and electronic states of tris(8-hydroxyquinoline) aluminum (Alq_3)/Al interfaces. (Miyamae et al. 2011) In OLEDs, Alq_3 is most widely used as electron transport/light emitting material. It is well known that Alq_3 has two possible geometrical isomers of meridional (C_1 symmetry) and facial (C_3 symmetry) forms, as shown in Fig. 1. In the meridional isomer, the three quinolate ligands around the central Al atom are not equivalent, while they are equivalent in the facial isomer. It has been reported that α- and amorphous Alq_3 consist of the meridional isomer, while γ- and δ-Alq_3 consist of facial isomer. (Nishiyama et al., 2009) Elucidating the electronic structures of the Alq_3/metal interface is required for its applicability to OLED. Such necessity should increase, due to the recent report of a significant enhancement of the current injection and OLED output induced by the insertion of an insulating layer such as LiF,(Hung et al., 1997) MgO, or MgF_2 (Shaheen et al., 1998) between the Al cathode and the Alq_3. Various mechanisms for this enhancement in the device efficiency have been proposed, and investigated using various techniques such as XPS, UPS, (Mason et al., 2001) and high resolution electron energy loss spectroscopy (HREELS). (He et al., 2000) One hypothesis is that thin LiF layer protects the Alq_3 from the deleterious reaction with Al.

Another hypothesis is that Li atoms produced by the dissociation of LiF by Al deposition lead to formation of the Alq_3 radical anion, is also considered. (Mason et al., 2001; Kido & Matsumoto 1998)

Figure 8 (a) shows the SFG spectra of 10 and 20 nm thick Alq_3 films on CaF_2 substrate excited by the visible light of 450 nm with the PPP polarization combination. In Fig. 8 (b), we compare the transmission IR spectrum of 69nm thick Alq_3 film deposited on CaF_2 substrate and the simulated IR spectrum for the Alq_3. The observed IR spectra of pristine Alq_3 agreed well with the IR spectrum of the meridional isomers in literature. (Kushto et al., 2000; Sakurai et al., 2004) The observed SFG spectra reasonably correspond to the IR spectrum in terms of the energies of the spectral features. Two peaks around 1600 cm^{-1} are derived from the C=C stretching modes of the quinolate ligands. The observed total SFG intensity of 20nm thick Alq_3 film shown in Fig. 8 was significantly larger than that of 10nm thick film, and the relative intensity of each peak also showed variation. We measure the SSP and PPP SFG spectra from 2 nm thick Alq_3 film deposited on CaF_2, however, the SFG signals derived from the Alq_3 were not observed.

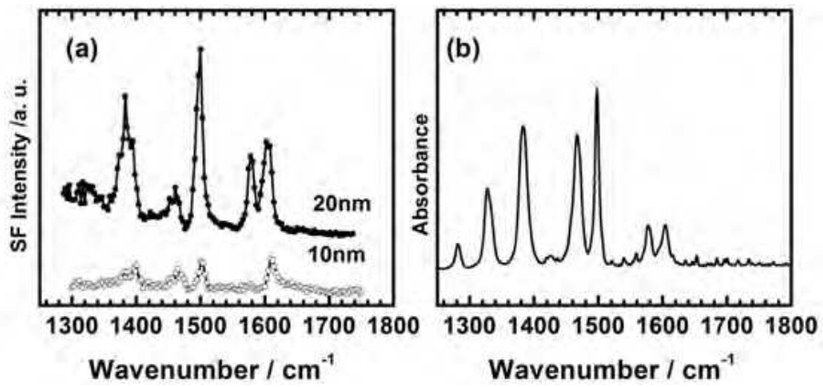

Fig. 8. (a) The SFG spectra of 10 and 20 nm thick Alq_3 on CaF_2 substrate excited by the visible light of 450 nm. (b) IR spectrum of 69 nm thick Alq_3 deposited on CaF_2 substrate.

In general, the growth of the SFG signal intensities with increasing the film thickness can be interpreted by the several reasons. First, the bulk SFG signal effect may come from the dipole-forbidden transitions. It is known that the dipole-forbidden transition observed in the SHG of the solid C_{60} films. (Koopmans et al., 1993; Kuhnke et al., 1998) Second-order nonlinearities of C_{60} are forbidden by symmetry under the electric-dipole approximation, but nonlocal bulk electric-quadrupole and magnetic-dipole processes appear due to its spherical character. However, such bulk contribution is not observed in the thickness dependence of the SHG on the photo-irradiated Alq_3 films. (Yoshizaki et al., 2005) Thus the bulk dipole-forbidden effects are excluded. Second, due to the existence of the two (air/Alq_3 and Alq_3/CaF_2) interfaces, the interference of the SFG signal between the two interfaces will induces the enhancements of the SFG signal intensities. The interference effects of the SFG signal due to the multiple layers are well analyzed by Hirose et al. (Hirose et al., 1998; Ishida et al., 1998) However, the SHG on the photo-irradiated Alq_3 films does not show such interference pattern. (Yoshizaki et al., 2005) Moreover, the decrease of in the intensity of the SHG signal was observed when the Alq_3 film was heated at a temperature lower than 100 °C. (Kajimoto et al., 2006) Although the part of the SFG signal might be influenced by the interference between the two interfaces, these SHG results suggest that the interference

effect is not the main origin of the increase of the signal intensities. We attributed that the growth of the SFG signal is due to the non-centrosymmetric orientation of the bulk film, as in the case of the ordered formic acid layers on the Pt. (Hirose et al., 1998) It has been reported that a large potential is built in as-deposited Alq_3 thick film in dark and it decays rapidly by exposure to the ambient light observed by the Kelvin probe method. (Yoshizaki et al., 2005; Ito et al., 2002) According to the Kelvin probe experiments, (Ito et al., 2002) the surface potential increased rapidly, in the initial stage of Alq_3 deposition up to 1 nm on Al substrate, corresponding to the formation of the interfacial dipole layer. (Seki et al., 1997) After the initial shift, the surface potential increased linearly over a wide range of thickness from 5 to 550 nm. And this behaviour is independent on the kind of the substrate. (Hayashi et al., 2004) For Alq_3, meridional isomer possesses permanent dipole moment. Thus the permanent dipole moment of Alq_3 makes a significant contribution to the surface potential when these dipoles align unidirectionally in the film. On the other hand, the large surface potential is rapidly reduced by exposure to ambient light. (Yoshizaki et al., 2005; Ito et al., 2002) At first, this was considered with the photo-induced randomization of molecular orientation, (Sugi et al., 2004) however, the first-order electroabsorption measurements for the Alq_3 confirms that the non-centrosymmetric molecular orientation remains even after the light irradiation, indicating that the reduction of the large surface potential is not caused by the orientation randomization. (Isoshima et al., 2009) It is also suggested that the orientation polarization of Alq_3 film is maintained in OLED structure even under light illumination after the device fabrication. (Noguchi et al., 2008)

To gain further information about the thickness dependent SFG signal intensities, in Fig. 9 we show the SFG spectra of the Alq_3 films deposited on Au substrate excited by the visible light of 450 nm with the PPP polarization combination. In this experiments, we used the Au precoated Si substrates instead of the CaF_2 in order to investigate how thickness the non-centrosymmetric orientation in the bulk films appears from. As shown in Fig. 9, the significant increase of the SFG signal intensities are observed from the range of the thickness from 5 to 20 nm. This observation clearly indicates that the thickness of more than 5 nm thick Alq_3 film has uniaxial dipole orientation, because the SFG process is allowed in non-centrosymmetric media. In these spectra, it should be noted that the SFG peak shapes also shows the thickness dependence. This behavior must be mainly comes from the decrease in the intensity of the non-resonant contributions from the Au. It is known that the intensity of the non-resonant term of the SFG is changed by the coverage of the surface. (Himmelhaus et al., 2000) In contrast, the SFG spectra of the 1, 2 and 5 nm thick Alq_3 films deposited on Au does not show the significant thickness dependence, and these spectra show almost the same shapes and the same intensities. Since the Alq_3 thickness of 1 nm is comparable to the average thickness of the Alq_3 monolayers, (Yokoyama et al., 2003) these results indicates that the observed SFG peaks mainly come from the Alq_3/Au interface, and the molecular orientation of the inside of the Alq_3 films from the range of the thickness from 1 to 5 nm does not show the preferred orientation in the bulk. This finding is consistent with the previously reported thickness and the substrate dependence of the surface potential measurements for the Alq_3 evaporated films. (Hayashi et al., 2004) This result is also suggestive that the SFG signals from air/Alq_3 interface is negligibly small than those from the Alq_3/Au interface. SFG signal contribution from the air/Alq_3 interface will be further discussed in the next section. Consequently, we conclude that the inside of the thin films of Alq_3 does not form the effective non-centrosymmetric molecular orientation except the Alq_3/Au interface in the case of the film thickness under 5 nm.

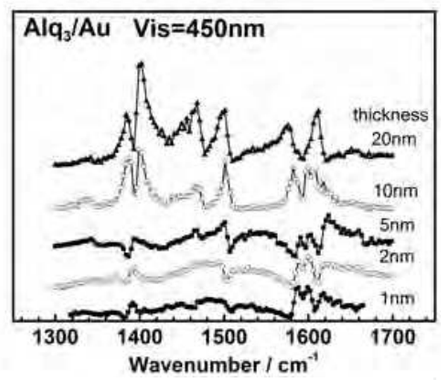

Fig. 9. Thickness dependence of the SFG spectra of Alq_3/Au.

As mentioned above, non-centrosymmetric orientation in the bulk films are remained even after the light irradiation, (Isoshima et al., 2009; Noguchi et al., 2008) while the surface potential observed in the Kelvin probe is rapidly reduced by the light-illumination. (Ito et al., 2002) The remaining of the molecular orientation on the bulk is consistent with our results of the thickness dependence of the SFG signal intensity. If the reduction of the surface potential is caused by the randomization of molecular orientation by the light-illumination, our probing lights should induce the randomization leading to much reduced SFG intensity and lack of thickness dependence in contrast to the observation, because the wavelength of the incident visible lights are near the absorption edge of Alq_3. Because the relation between the permanent dipole of the meridional Alq_3 and the vibrational transition dipole is not known, the mechanism for the appearance of the large surface potential in Alq_3 thick film is not elucidated by our SFG measurements. However, we conclude that the Alq_3 molecules spontaneously orient and form non-centrosymmetric orientation in the bulk even after the light irradiation in the case of the film thicknesses more than 5 nm.

4.2.2 DR-SFG study of Alq_3 thin films deposited on Al

In Fig. 10 we show the SFG vibrational spectra of the 2 nm thick Alq_3 deposited on Al with various visible wavelength in a PPP polarization (P-, P-, and P-polarized for SFG, visible, and IR, respectively) combination measured in the ambient condition. To minimize the influence of the air, the Alq_3 was covered with the 50 nm thick CaF_2. The SFG spectra of the 1 nm thick Alq_3/Al show almost the same to that of the 2 nm thick one. Since the film thickness of 1 nm is comparable to the average thickness of the Alq_3 monolayers, the observed SFG spectra of 2 nm thick Alq_3/Al are mainly originated from the Alq_3/Al interface. The 1 nm thick data is unstable and much worse reproducibility. On the other hand, the SFG spectra of the 5 nm thick Alq_3/Al systems show relatively stronger signals than those of the 1 and 2 nm thick Alq_3/Al. Such thickness dependent signal enhancements must be due to the effect of the uniaxial orientation of the molecular dipole, as mentioned in the preceding section. In order to minimize the effect of the uniaxial orientation, we used the 2 nm thick Alq_3 films for the SFG measurements. In the SFG spectra of the CaF_2/Alq_3/Al shows the bands at 1344, 1386, 1426, 1465, 1504, 1583, and 1612 cm^{-1}. The bands at 1583 and 1612 cm^{-1} are derived from the C=C stretching modes of the quinolate ligands. (Kushto et al., 2000; Sakurai et al., 2004) As shown in Fig. 10, remarkable changes in intensity of these peaks can be clearly observed by changing the visible wavelength. Figure 10 (b) shows the changes in the two representative peak strengths (A_l) of the peaks deduced from the fitting

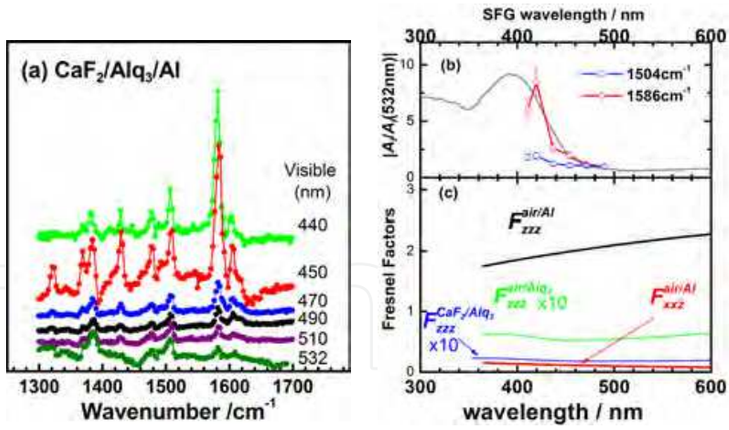

Fig. 10. (a) The SFG spectra of the Alq_3 on Al with various visible wavelengths. Spectra are offset for clarity. (b) Changes in the peak strengths of the 1583 and 1504 cm^{-1} as a function of the photon energies of the SFG. Optical absorption spectrum of the Alq_3 film is also shown by gray line. (c) Evolution of the Fresnel factors of F_{zzz} (black line) and F_{xxz} (red line) for the air/Al, F_{zzz} for the air/Alq_3 (green line), and F_{zzz} for the CaF_2/Alq_3 (blue line) interfaces. The F_{zzz}^{air/Alq_3} and $F_{zzz}^{CaF_2/Alq_3}$ are multiplied by 10.

of the DR-SFG spectra in Fig. 10 (a) using eq. (4) as a function of the photon energies of the SFG. In order to observe the enhancement ratios of the peak strength with the output SFG frequencies, the peak strengths are normalized with the strength of the SFG spectrum taken at the visible wavelength of 532 nm. For comparison, we show the optical absorption spectrum of the 20 nm thick Alq_3 film on CaF_2 in Fig. 10 (b). The excitation spectra exhibit a resonance almost coincident with the absorption spectrum for the Alq_3 thin film. Especially, significant increase in intensity is observed for the band at 1583 cm^{-1}. In contrast, the enhancements ratio of the SFG peak strength of the band at 1504 cm^{-1} is relatively weaker than that of the bands at 1583 cm^{-1}. These vibrational mode around 1583 cm^{-1} is assigned to the C=C stretching of the quinolate group while the 1504cm^{-1} peak is mixed modes that contain the contributions from the C-C and C-H in-plane bending motions. (Kushto et al., 2000) They are expected to have different degrees of coupling with the electronic transition. For Alq_3, the electronic transition at 390 nm is dominated by the π-π* excitation of the quinolate ligands. (Halls & Schlegel 2001) Thus it is reasonable that the C=C stretching of the quinolate ligands are effectively enhanced due to the resonance with the π-π* transitions. The SFG electronic excitation spectra in Fig. 10 (b) are slightly shifted to lower frequency as compared to the optical absorption spectrum of the Alq_3. The shift of the electronic transition peak may be suggestive that the electronic excitation gap at the interface becomes smaller than that of the bulk. Since the SFG excitation spectra are not measured in the whole region across the optical transition peak, and therefore, further experiments with the shorter wavelength excitation are needed to reveal the definitive information of the excitation profiles at the interface.

For the analysis of the doubly-resonant SFG, it should be important to note that the changes of the Fresnel factors have to be considered since it might change with the variation of the visible wavelength. The effective the second-order nonlinear susceptibility tensor components of an azimuthally isotropic sample contributes to the PPP SFG signals can be written as

$$\begin{aligned} A_{q,PPP} = & -L_{xx}(\omega_{SF})L_{xx}(\omega_{VIS})L_{zz}(\omega_{IR})\cos\beta_{SF}\cos\beta_{VIS}\sin\beta_{IR}\chi_{xxz} \\ & - L_{xx}(\omega_{SF})L_{zz}(\omega_{VIS})L_{xx}(\omega_{IR})\cos\beta_{SF}\sin\beta_{VIS}\cos\beta_{IR}\chi_{xzx} \\ & + L_{zz}(\omega_{SF})L_{xx}(\omega_{VIS})L_{xx}(\omega_{IR})\sin\beta_{SF}\cos\beta_{VIS}\cos\beta_{IR}\chi_{zxx} \\ & + L_{zz}(\omega_{SF})L_{zz}(\omega_{VIS})L_{zz}(\omega_{IR})\sin\beta_{SF}\sin\beta_{VIS}\sin\beta_{IR}\chi_{zzz} \end{aligned}, \quad (7)$$

where $L_{xx}(\omega)$ and $L_{zz}(\omega)$ are the Fresnel coefficients at frequency ω, β_{SF}, β_{VIS}, and β_{IR} are the reflection angles of the sum frequency, visible, and IR pulses, respectively; and χ_{ijk}s are the nonvanishing elements of the second-order nonlinear susceptibility. (Zhuang et al., 1999) We found that χ_{xzx} and χ_{zxx} are much smaller than χ_{xxz} and χ_{zxx}. Thus the Fresnel factors $F_{zzz} = \left|L_{ZZ}(\omega_{SF})L_{ZZ}(\omega_{VIS})L_{ZZ}(\omega_{IR})\sin\beta_{SF}\sin\beta_{VIS}\sin\beta_{IR}\right|$ and $F_{xxz} = \left|L_{XX}(\omega_{SF})L_{XX}(\omega_{VIS})L_{ZZ}(\omega_{IR})\cos\beta_{SF}\cos\beta_{VIS}\sin\beta_{IR}\right|$ were calculated using the complex refractive indices of metallic aluminum. (Parik, 1985) As shown in Fig. 10 (b), the F_{zzz} at air/Al interface monotonically decreases with the increase of the photon energy of the SFG, and it does not explain the evolution of the SFG intensities of the Alq_3/Al. Thus we conclude that the changes of the Fresnel factors do not much affect on the spectral shape of the SFG excitation profile of the Alq_3/Al.

The analysis of the Fresnel factor is also important for the investigation of such a thin layered sample. We calculated the Fresnel factors F_{zzz} at air/Alq_3 and CaF_2/Alq_3 interfaces, assuming that the air/Alq_3 interface is azimuthally isotropic. The wavelength dependence of the refractive indices for Alq_3 were used for the evaluation of the Fresnel factors at air/Alq_3 and CaF_2/Alq_3 interfaces. (Djurišić et al., 2002) As shown in Fig. 10 the F_{zzz} at air/Alq_3 and CaF_2/Alq_3 interfaces are much smaller than the F_{zzz} at air/Al interface. From this observation, we conclude that the experimentally observed SFG should be mainly from the Alq_3/Al interface.

In the previous UPS study of the Alq_3 deposited on Al systems, an extra occupied state above the HOMO level was detected, suggesting a strong chemical interaction between Alq_3 and Al. (Yokoyama et al., 2003) It was suggested that the interaction between Al and Alq_3 is somewhat different from the charge transfer as reported for alkaline metal doped Alq_3. (Curioni & Andreoni, 1999) On the other hand, a theoretical calculation of Alq_3 layer on Al (111) suggested that the interfacial interaction is weak, (Yanagisawa & Morikawa 2006) These previous findings are controversial and not easy to discuss consistently, but one possible reason of this discrepancy must be due to the least reactivity of the clean Al(111) surface used in the DFT. (Yanagisawa & Morikawa 2008) If the strong chemical interaction occurs at the interface, the vibrational SFG spectra and the corresponding electronic excitation profiles should provide different behavior to those of the bulk. On the contrary, the SFG excitation profile of the 1583 cm^{-1} band is almost identical to the visible optical absorption spectrum of the pristine Alq_3, and we cannot find such spectral changes. Although the electronic excitation profile does not show significant changes, however, the position of the C=C stretching peak shows slightly red-shifted. As discussed below, red-shift of the C=C peak is indicative of the charge transfer from the Al substrate to Alq_3.

4.2.3 DR-SFG study of Al layer deposited onto Alq_3

The traditional surface analysis techniques such as UPS have been applied to examine the interfaces formed by depositing organic material on metals, which are not much troubled by the factor of chemical reaction. (Ishii et al., 1999) Actually, in many cases the UPS spectra of

organic-on-metal systems show only rigid shifts on the energy scale, suggesting the absence of strong chemical interaction. In contrast, actual OLEDs are fabricated by organic layers sandwiched by a cathode and anode. The buried interface between metal anode and the organic layer is formed by the deposition of the metal on organic materials. When the metal is deposited on an organic layer by evaporation, the high reactivity of the vaporized hot metal atom often leads to a chemical reaction at the interface, and diffuse into the organic layer. Due to the energy transfer from the hot metal atom, deposition of the metal on organic materials may also induce the decomposition of the molecules, polymerization of the molecules, reorientation of the molecules, desorption of the organic materials from the substrate, and so on. Thus the "*metal-on-organic*" systems are generally much more complex than the organic-on-metal systems. Due to the high reactivity of the Al atom, reactions between the Alq_3 and Al are expected by the deposition of the Al layer. For the characterization of the buried metal-on-organic interface, next, we measure the SFG spectra for the Al deposited on Alq_3 film. The deposited thick Al layer can act as superior gas barrier, and the extent of the oxidation of the Al interface is much reduced.

In Fig. 11, we show the SFG spectra of Al film directly deposited on 5nm thick Alq_3 film on CaF_2 substrate with various visible wavelengths in a PPP polarization. In the case of the Al/Alq_3/CaF_2 system, the thickness of Alq_3 is set to 5 nm. When we use the Alq_3 layer of 2 nm thick sandwiched by CaF_2 and Al, the SFG gives quite weak signal. Low sticking probability of the Alq_3 on CaF_2 is not plausible judging from the molecular weight of Alq_3. Although the exact reason is not clear at this present, we tentatively thought that the detectable interface could not be formed by the deposition of the 2 nm thick Alq_3. As mentioned above, the metal atoms often diffuse into the organic layer, and this process may prevent to form the clear interface for the 2 nm thick Alq_3 sandwiched between CaF_2 and Al. It should be noted that the SFG signal comes mainly from the Al/Alq_3 interface, not from the Alq_3/CaF_2 interface, because no SFG signals are detected from the thin Alq_3 layer deposited on CaF_2. This is further supported by the Fresnel factor difference between Al and CaF_2 interfaces. We show in Fig. 10 (b), the F_{zzz} at CaF_2/Alq_3 interface are negligibly smaller

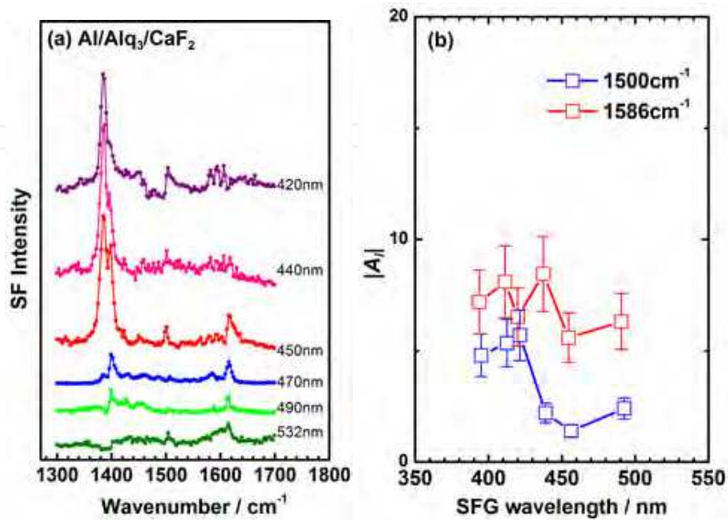

Fig. 11. (a) The SFG spectra of Al/Alq_3/CaF_2 substrate. (b) Changes in the peak strengths of the 1586 and 1500 cm^{-1} of the SFG spectra as a function of the photon energies of the SFG.

than F_{zzz} at air/Al interface. One may think that the SFG spectra in Fig. 11 are comes from the Alq_3 bulk, since the thick Alq_3 film shows uniaxial orientation. Although the evaluation of the bulk contribution needs transmission experiments, (Wei et al., 2000) if the SFG signals in Fig. 11 are mainly originated from the bulk Alq_3, the spectral shapes and their behavior should be similar to those of the Alq_3 on Al systems. Therefore, we thought that the main contribution of the SFG signals is the Al/Alq_3 interface.

The spectral features are different from the SFG spectra of Alq_3/Al and the pristine IR spectrum of the Alq_3. The relative intensities of bands derived from the C=C stretching around 1600 cm^{-1} becomes weak as compared to the case of the Alq_3/Al. Figure 11 (b) shows the changes in the two representative peak strengths (A_l) of the vibrational peaks deduced from the fitting of the DR-SFG spectra in Fig. 11 (a) as a function of the photon energies of the SFG. As shown in Fig. 11 (b), the SFG electronic profiles derived from the C=C bands does not agree with the linear optical absorption spectrum of the Alq_3, indicating that the electronic-resonant effects associated with the π-π* transitions in the quinolate rings are almost vanished. According to the theoretical calculations for the Al-Alq_3 complex, the energy diagrams near the gaps are significantly changed by the chemical bonding formation between Al and Alq_3. (Curioni & Andreoni, 1999) In contrast to the case of the alkaline-metal-Alq_3 complex, HOMO of pristine Alq_3 is destabilized by the interaction with the Al 3s orbital. The interaction with the Al is such that one of the Alq_3 HOMOs is repelled to higher energy, and a state with predominant Al character appears in the same energy range. Al-Alq_3 interaction also induces the modification of LUMO. Previous NEXAFS study of Al/Alq_3 interface suggests that the Al-Alq_3 interaction is not simple electron transfer from Al to Alq_3. (Yokoyama et al., 2005) Although the theoretical simulations for the 1:1 Al-Alq_3 complex cannot predict the observed NEXAFS results, modification of HOMO (LUMO) level occurs at the Al/Alq_3 interface. Thus we conclude that disappearance of the doubly-resonant effect associated with the π-π* transitions must be caused by the perturbation of the HOMO and LUMO of Alq_3 by the interaction of the Al.

4.2.4 Effects of the LiF insertion between Al and Alq_3

In this section, we discuss the effects of the insertion of a LiF layer between Al and Alq_3 interface. The SFG spectra of the Al/LiF/Alq_3 system with various visible wavelengths in a PPP polarization are shown in Fig. 12 (a). The spectral features are quite different from those of Alq_3/Al and Al/Alq_3. The new broad bands, which show the weak excitation wavelength dependence, appear around 1335 and 1450 cm^{-1}. The C=C stretching modes of the quinolate ligands are observed at 1572 and 1607 cm^{-1}. The frequency shift to lower wavenumber of the C=C stretching mode is also reported in the IR and DFT study of the potassium-doped Alq_3. (Sakurai et al., 2004) The DFT calculations and the IR spectrum for the potassium-doped Alq_3 suggested that the C=C stretching frequency of Alq_3 anion is lower than that of pristine Alq_3 molecule. Consequently, the red-shift of the C=C stretching bands in the SFG spectra is indicative of the formation of the Alq_3 anionic states upon reaction with Li at the interface. (Mason et al., 2001) This observation is in good agreement with the previous UPS and XPS measurements for the Al/LiF/Alq_3 interfaces (Mason et al., 2001; Ding et al., 2009) and, to our knowledge, this is the first observation of the anionic state formation at the buried interface in ambient condition. Figure 12 (b) shows the SFG excitation profiles obtained from the DR-SFG spectra in Fig. 12 (a) as a function of the photon energies of the SFG. The SFG

excitation profiles derived from the 1572 cm^{-1} band gives maximum around 420 nm, however, it does not show large shift to the lower photon energy. If the Alq_3 at the LiF interface forms the Alq_3 anion, the absorption peaks should appear below 600 nm. (Ganzorig & Fujihira, 2002) The charges transferred from the Li might smear the SFG excitation profiles of the C=C stretching. Unfortunately, our SFG system cannot generate the sufficient power of the light below 640 nm at present. Further experiments with the longer wavelength excitation will reveal the electronic character at the charged interface.

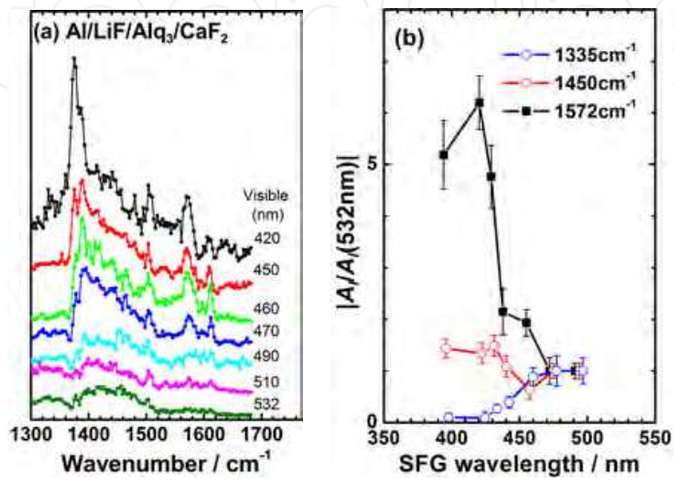

Fig. 12. (a) The SFG spectra of Al/LiF/Alq_3. (b) The changes in the peak strengths of the three representative vibrational peaks as a function of the photon energies of the SFG.

Next, we mention the origin of the broad peaks at 1335 and 1450 cm^{-1}. Similar broad features are observed by IR and Raman studies of potassium-doped Alq_3 and the Al/LiF/Alq_3 system. (Sakurai et al., 2004) It was suggested that these bands are derived from the quinolate ligands reacted with potassium or lithium. On the other hand, recent Raman studies performed in UHV environment show the similar broad features around 1355, 1405, and 1560 cm^{-1} for Alq_3/Al system, and 1315, 1435, and 1515 cm^{-1} for Alq_3/Ca system, respectively. (Davis & Pemberton, 2008, 2009) They assigned these modes are derived from the G-bands and the D-bands of the graphitic carbon generated by the deposition of Ca or Al onto Alq_3 thick film. One may think that the graphite related bands are IR inactive modes, however, these modes become IR active in the nitrogenated amorphous graphite. (Kaufman et al., 1989) NEXAFS studies also suggest the existence of the chemical interaction different from electron transfer at the Al/LiF/Alq_3 system, which differs from Al/Alq_3 and Li/Alq_3 interfaces. (Yokoyama et al., 2005) Although further studies are necessary to determine the origin of these broad features, the wavelength independent SFG excitation profiles of these features may be suggestive that these bands are originated from the graphite-like bands, not from the Alq_3. On the other hands, the red-shift of the other SFG peaks, which shows the remarkable wavelength dependent SFG excitation profiles, may be indicative by the formation of the Alq_3 anionic states at the interface, as mentioned above. Because the interface formed by the metal deposition onto the organic materials is much more complicated than the organic-on-metal system, we conclude that the Al/LiF/Alq_3 buried interface might be co-existence of the negatively charged Alq_3 by the charge transfer from the Li and the Li-reacted graphitic carbon-like Alq_3.

Finally, we discuss the interfacial vibrational and electronic structural difference between Al/Alq_3 and Al/LiF/Alq_3 interfaces by comparing with the SFG spectra. Figure 13 shows the SFG spectra of the Alq_3/Al, Al/Alq_3, and Al/LiF/Alq_3 systems excited by the visible light of 450 nm with the PPP polarization combination. From these data, we can confirm three differences by the different interface. First, the red-shift of the C=C stretching modes are observed in the Al/LiF/Alq_3 interfaces, while such shift is not observed in the case of the Al/Alq_3 system. These spectral behaviors clearly indicate that the chemical interaction between Li and Alq_3 occurred at the Al/LiF/Alq_3 interface. Red-shift of the SFG vibrational modes is suggestive to the formation of the Alq_3 anionic states at the interface. Second, the electronic-resonance for the C=C stretching modes are vanished for the Al/Alq_3 system, while it remains in the case of the Al/LiF/Alq_3 system. This observation indicates that the energy diagrams near the band gaps are modified by the chemical reaction between Al and Alq_3, rather than the simple charge transfer from Al to Alq_3. Finally, the broad features which might be due to the graphite-like carbon are observed in the case of the Al/LiF/Alq_3 system. Insertion of the LiF layer between Al and Alq_3 induces reaction at the interface, and it emerges the negatively charged Alq_3 and the Li-reacted graphitic carbon-like Alq_3.

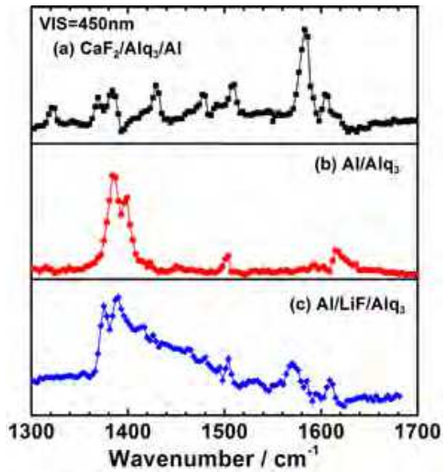

Fig. 13. The SFG spectra of the (a) CaF_2/Alq_3/Al, (b) Al/Alq_3, and (c) Al/LiF/Alq_3 systems excited by the visible light of 450 nm with the PPP polarization combination.

5. Conclusion

The interfacial vibrational and electronic states of organic/metal interfaces were studied using doubly-resonant SFG spectroscopy. In the SFG studies of the air/PFO and the Al/LiF/PFO interfaces, the planes of PFO rings are nearly parallel to the surface plane at the air/PFO interface. This planar orientation induced by the interface confinement effects leads to the smaller band gaps at the air/PFO and the Al/LiF/PFO interfaces than those of the bulk PFO. In the DR-SFG spectra of the Alq_3/Al, remarkable changes in intensities of the SFG peaks derived from the C=C stretching of the quinolate ligands can be clearly observed by changing the visible wavelength due to the double resonance effect. In contrast, The SFG excitation profiles of the C=C stretching of the Al/Alq_3 interfaces do not show the wavelength dependences, indicating that the perturbation of the HOMO and LUMO of pristine Alq_3 by the interaction of the Al. The SFG spectra of the Al/LiF/Alq_3 system

indicates that the existence of the Alq_3 anionic states at the buried interface in atmospheric condition. Additional broad bands around 1335 and 1450 cm^{-1} might be due to the existence of the Li-reacted graphitic carbon-like Alq_3. Co-existence of the negatively charged Alq_3 and the Li-reacted graphitic carbon-like Alq_3 at the buried interface is proposed.

Although the experimental results obtained here were performed in ambient condition, the present study lead to a better understanding of the molecular and the electronic structure of the organic/metal interfaces. In much the same way as multi-dimensional spectroscopy is suitable for studies of intra- and inter-molecular interactions in the bulk, the DR-SFG provides a similar opportunity for studies of molecules at interfaces. This doubly-resonant SFG technique, which was proved feasible for OLEDs study in this chapter, offers a novel spectroscopy for the characterization of the vibrational and electronic structures at the buried organic interfaces.

6. Acknowledgments

The work in this paper was performed in collaboration with Professors H. Ishii, Y. Ouchi, and K. Seki, and Drs W. Mizutani, K. Tsukagoshi, Y. Noguchi, E. Ito, and Y. Sakurai; all are gratefully acknowledged. We gratefully acknowledge financial support from the Mitsui Chemicals Inc. This work was supported in part by Grants-in-Aid for Scientific Research from the Japan Society for the Promotion of Science (JSPS) of Japan.

7. References

Ariu, M.; Lidzey, D. G.; Bradley, D. D. C., Influence of film morphology on the vibrational spectra of dioctyl substituted polyfluorene (PFO), S*ynth. Met.*, Vol. 111 (2000), pp. 607-610.

Becker, K.; Lupton, J. M., Dual species emission from single polyfluorene molecules: signatures of stress-induced planarization of single polymer chains, *J. Am. Chem. Soc.*, Vol. 127, No. 20 (2005), pp. 7306-7307.

Burroughes, J. H.; Bradley, D. D. C.; Brown, A. R.; Marks, R. N.; Mackay, K.; Friend, R. H.; Burn, P. L.; Holmes, A. B., Light-emitting diodes based on conjugated polymers, *Nature*, Vol. 347, No. 6293 (1990), pp. 539-540.

Cadby, A. J.; Lane, P. A.; Mellor, H.; Martin, S. J.; Grell, M.; Giebeler, C.; Bradley, D. D. C.; Wohlgenannt, M.; An, C.; Vardeny, Z. V., Film morphology and photophysics of polyfluorene, *Phys. Rev. B*, Vol. 62, No. 23 (2000), 62, pp. 15604-15609.

Campoy-Quiles, M.; Heliotis, G.; Xia, R.; Ariu, M.; Pintani, M.; Etchegoin, P.; D. D. C. Bradley, D. D. C., Ellipsometric characterization of the optical constants of polyfluorene gain media, *Adv. Func. Mater.*, Vo. 15, No. 6 (2005), pp. 925-933.

Cheum, H.; Galbrecht, F.; Nehls, B.; Scherf, U.; Winokur, M. J., Interface specific variations in the steady-state optical properties of polyfluorene thin films, *J. Mater. Sci.: Mater. Electronics*, Vol. 20, Supplement 1 (2009), S498-S504.

Curioni, A.; Andreoni, W., Metal−Alq_3 complexes: The nature of the chemical bonding, *J. Am. Chem. Soc.*, Vol. 121, No. 36 (1999), pp. 8216-8220.

Davis, R. J.; Pemberton, J. E., Investigation of the interfaces of tris-(8-hydroxyquinoline) aluminum with Ag and Al using surface Raman spectroscopy, *J. Phys. Chem. C*, Vo. 112, No. 11 (2008), pp. 4364-4371.

Davis, R. J.; Pemberton, J. E., Surface Raman spectroscopy of chemistry at the tris(8-hydroxyquinoline) aluminum/Ca interface, *J. Phys. Chem. A*, Vol. 113, No. 16 (2009), pp. 4397-4402.

Ding, H.; Park, K.; Gao, Y.; Kim, D. Y.; So, F., Electronic structure and interactions of LiF doped tris-(8-hydroxyquinoline) aluminum (Alq), *Chem. Phys. Lett.*, Vol. 473, Nos. 1-3 (2009), pp. 92-95.

Djurišič, A. B.; Kwong, C. Y.; Guo, W. L.; Lau, T. W.; Li, E. H.; Liu, Z. T.; Kwok, H. S.; Lam, L. S. M.; Chan, W. K., Spectroscopic ellipsometry of the optical functions of *tris*-(8-hydroxyquinoline) aluminum (Alq_3),*Thin Solid Films*, Vol. 416, Nos. 1-2 (2002), pp. 233-241.

Ganzorig, C.; Fujihira, M., A possible mechanism for enhanced electrofluorescence emission through triplet–triplet annihilation in organic electroluminescent devices, *Appl. Phys. Lett.*, Vol. 81, No 17 (2002), pp. 3137-3179.

Gong, X.; Iyer, P. K.; Moses, D.; Bazon, G. C.; Heeger, A. J.; Xiao, S. S., Stabilized blue emission from polyfluorene-based light-emitting diodes: Elimination of fluorenone defects, *Adv. Func. Mater.*, Vol. 13, No. 4 (2003), pp. 325.

Grell, M.; Bradley, D. D. C.; Ungar, G.; Hill, J.; Whitehead, K. S., Interplay of physical structure and photophysics for a liquid crystalline polyfluorene, *Macromolecules*, Vol. 32, No. 18 (1999), pp. 5810-5817.

Halls, M. D.; Schlegel, H. B., Molecular orbital study of the first excited state of the OLED material tris-(8-hydroxyquinoline)aluminum(III), *Chem. Mater.*, Vol. 13, No. 8 (2001), pp. 2632-2640.

Hayashi, M.; Lin, S. H.; Raschke, M. B.; Shen, Y. R., A Molecular theory for doubly resonant IR−UV-vis sum-frequency generation, *J. Phys. Chem. A*, Vol. 106, No. 10 (2002), pp. 2271-2282.

Hayashi, N.; Imai, K; Suzuki, T.; Kanai, K.; Ouchi, Y.; Seki, K., Substrate dependence of giant surface potential of Alq_3 and the examination of surface potential of related materials, *Proceedings of International Symposium on Super-Functionality Organic Devices*, IPAP Conf. Series 6, pp. 69-72, ISBN4-900526-20-7 Chiba, October, 2004.

He, P.; Au, F. C. K.; Wang, Y. M.; Cheng, L. F.; Lee, C. S.; Lee, S. T., Direct evidence for interaction of magnesium with tris(8-hydroxy-quinoline) aluminum, *Appl. Phys. Lett.*, Vol. 76, No. 11 (2000), pp. 1422-1424.

Himmelhaus, M.; Eisert, F.; Buck, M.; Grunze, M., Self-assembly of *n*-alkanethiol monolayers; A study by IR−visible sum frequency spectroscopy (SFG), *J. Phys. Chem. B*, Vol. 104, No. 3 (2000), pp. 576-584.

Hirose, C.; Ishida, H.; Iwatsu, K.; Watanabe, N.; Kubota, J.; Wada, A.; Domen, K., In situ SFG spectroscopy of film growth. I. General formulation and the analysis of the signal observed during the deposition of formic acid on Pt(110)-(1×2) surface, *J. Chem. Phys.*, Vol. 108, No. 14 (1998), pp. 5948-5956.

Hung, L. S.; Tang, C. W.; Mason, M. G., Enhanced electron injection in organic electroluminescence devices using an Al/LiF electrode, *Appl. Phys. Lett.*, Vol. 70, No. 2 (1997), pp. 152-154.

Ishida, H.; Iwatsu, K.; Kubota, J.; Wada, A.; Domen, K.; Hirose, C., *In situ* SFG spectroscopy of film growth. II. Deposition of formic acid on Ni(110) surface, *J. Chem. Phys.*, Vol. 108, No. 14 (1998), pp. 5957-5964.

Ishii, H.; Sugiyama, K.; Ito, E.; Seki, K., Energy level alignment and interfacial electronic structures at organic/metal and organic/organic interfaces, *Adv. Mater.*, Vol. 11, No. 8 (1999), pp. 605-625.

Isoshima, T.; Ito, H.; Ito, E.; Okabayashi, Y.; Hara, M., Long-term relaxation of molecular orientation in vacuum-deposited Alq_3 thin films, *Mol. Cryst. Liq. Cryst.*, Vol. 505, No. 1 (2009), pp. 59-63.

Ito, E.; Washizu, Y.; Hayashi, N.; Ishii, H.; Matsuie, N.; Tsuboi, K.; Harima, Y.; Yamashita, K.; Seki, K., Spontaneous buildup of giant surface potential by vacuum deposition of Alq_3 and its removal by visible light irradiation, *J. Appl. Phys.*, Vol. 92, No. 12 (2002), pp. 7306-7310.

Iwahashi, T.; Miyamae, T.; Kanai, K.; Seki, K.; Kim, D.; Ouchi, Y., Anion configuration at the air/liquid interface of ionic liquid [bmim]OTf studied by sum-frequency generation spectroscopy, *J. Phys. Chem. B*, Vol. 112, No. 38 (2008), pp. 11936-11941.

Kajimoto, N.; Manaka, T.; Iwamoto, M., Decay process of a large surface potential of Alq_3 films by heating, *J. Appl. Phys.*, Vol. 100, No. 5 (2006), pp. 053707.

Kaufman, J. H.; Metin, S.; Saperstein, D. D., Symmetry breaking in nitrogen-doped amorphous carbon: Infrared observation of the Raman-active *G* and *D* bands, *Phys. Rev. B*, Vol. 39, No. 18 (1989), pp. 13053-13060.

Kawana, S.; Durrel, M.; Lu, J.; Macdonald, J. E.; Grell, M.; Bradley, D. D. C.; Jukes, P. C.; Jones, R. A. L.; Bennett, S. L., X-ray diffraction study of the structure of thin polyfluorene films, *Polymer*, Vol. 43, No. 6 (2002), pp. 1907-1913.

Kido, J.; Matsumoto, T., Bright organic electroluminescent devices having a metal-doped electron-injecting layer, *Appl. Phys. Lett.*, Vol. 73, No. 20 (1998), pp. 2866-2868.

Knaapila, M.; Lyons, B. P.; Kisko, K.; Foreman, J. P.; Vainio, U.; Mihaylova, M.; Seeck, O. H.; Palsson, L. O.; Serimaa, R.; Torkkeli, M.; Monkma, A. P., X-ray diffraction studies of multiple orientation in poly(9,9-bis(2-ethylhexyl)fluorene-2,7-diyl) thin films, *J. Phys. Chem. B*, Vol. 107, No. 45 (2003), pp. 12425-12430.

Koopmans, B.; Janner, A.-M.; Jonkman, H. T.; Sawatzky, G. A.; van der Woude, F., Strong bulk magnetic dipole induced second-harmonic generation from C_{60}, *Phys. Rev. Lett.*, Vol. 71, No. 21 (1993), pp. 3569-3572.

Kuhnke, K.; Epple, M.; Kern, K., Second-harmonic spectroscopy of fullerenes, *Chem. Phys. Lett.*, Vol. 294, Nos. 1-3 (1998), pp. 241-247.

Kushto, G. P.; Iizumi, Y.; Kido, J.; Kafafi, Z. H., A matrix-isolation spectroscopic and theoretical investigation of tris(8-hydroxyquinolinato)aluminum(III) and tris(4-methyl-8-hydroxyquinolinato)aluminum(III), *J. Phys. Chem. A*, Vol. 104, No. 16, (2000), pp. 3670-3680.

Li, Q.; Hua, R.; Chou, K. C., Electronic and conformational properties of the conjugated polymer MEH-PPV at a buried film/solid interface investigated by two-dimensional IR−visible sum frequency generation, *J. Phys. Chem. B*, Vol. 112, No. 8 (2008), pp. 2315-2318.

List, E. J. W.; Guentner, R., The effect of keto defect sites on the emission properties of polyfluorene-type materials, *Adv. Mater.*, Vol. 14, No. 5, (2002), pp. 374-378.

Mallavia, R.; Montilla, F.; Pastor, I.; Velasquez, P.; Arredondo, B.; Alvarez, A. L.; Mateo, C. R., Characterization and side chain manipulation in violet-blue poly-[(9,9-dialkylfluoren-2,7-diyl)-*alt*-co-(benzen-1,4-diyl)] backbones, *Macromolecules*, Vol. 38, No. 8 (2005), pp. 3185-3192.

Mason, M. G.; Tang, C. W.; Hung, L. –S.; Raychaudhuri, P.; Madathi, J.; Giesen, D. J.; Yan, L.; Le, Q. T.; Gao, Y.; Lee, S. –T.; Liao, L. S.; Cheng, L. F.; Salaneck, W. R.; dos Santos, D. A.; Brédas, J. L., Interfacial chemistry of Alq_3 and LiF with reactive metals, *J. Appl. Phys.*, Vol. 89, No. 5 (2001), pp. 2756-2765.

Miyamae, T.; Nozoye, H., Correlation of molecular conformation with adhesion at AlO_x/poly(ethylene terephthalate) interface studied by sum-frequency generation spectroscopy, *Appl. Phys. Lett.*, Vol. 85, No. 19 (2004), pp. 4373-4375 (2004).

Miyamae, T.; Akiyama, H.; Yoshida, M.; Tamaoki, N., Characterization of poly(*N*-isopropylacrylamide)-grafted interfaces with sum-frequency generation spectroscopy, *Macromolecules*, Vol. 40, No. 13 (2007), pp. 4601-4606.

Miyamae, T.; Morita, A.; Ouchi, Y., First acid dissociation at an aqueous H_2SO_4 interface with sum frequency generation spectroscopy, *Phys. Chem. Chem. Phys.*, Vol. 10, No. 15 (2008), pp. 2010-2013.

Miyamae, T.; Miyata, Y.; Kataura, H., Two-color sum-frequency generation study of single-walled carbon nanotubes on silver, *J. Phys. Chem. C*, Vol. 113, No. 34, (2009), pp. 15314-15319.

Miyamae, T.; Tsukagoshi, K.; Mizutani, W., Two-color sum frequency generation study of poly(9,9-dioctylfluorene)/electrode interfaces, *Phys. Chem. Chem. Phys.*, Vol. 12, No. 44 (2010), pp. 14666-14669.

Miyamae, T.; Ito, E.; Noguchi, Y.; Ishii, H., Characterization of the interactions between Alq_3 thin films and Al probed by two-color sum-frequency generation spectroscopy, *J. Phys. Chem. C*, Vol. 15, No. 19 (2011), pp. 9551-9560.

Montilla, F.; Mallavia, R., On the origin of green emission bands in fluorene-based conjugated polymers, *Adv. Func. Mater.*, Vol. 17, No. 1 (2007), pp. 71-78.

Nishiyama, Y.; Fukushima, T.; Takami, K.; Kusaka, Y.; Yamazaki, T.; Kaji, H., Characterization of local structures in amorphous and crystalline tris(8-hydroxyquinoline) aluminum(III) (Alq_3) by solid-state ^{27}Al MQMAS NMR spectroscopy, *Chem. Phys. Lett.*, Vol. 471, Nos. 1-3 (2009), pp. 80-84.

Noguchi, Y.; Sato, N.; Tanaka, Y.; Nakayama, Y.; Ishii, H., Threshold voltage shift and formation of charge traps induced by light irradiation during the fabrication of organic light-emitting diodes, *Appl. Phys. Lett.*, Vol. 92, No. 20 (2008), pp. 203306.

Parik, E. D., Ed. *Handbook of Optical Constants of Solids*, 1985, Academic Press, ISBN 0-12-544420-6, London.

Raschke, M. B.; Hayashi, M.; Lin, S. H.; Shen, Y. R., Doubly-resonant sum-frequency generation spectroscopy for surface studies, *Chem. Phys. Lett.*, Vol. 359, Nos. 5-6 (2002) pp.367-372.

Sakurai, Y.; Hosoi, Y.; Ishii, H.; Ouchi, Y.; Salvan, G.; Kobitski, A.; Kampen, T. U.; Zahn, D. R. T.; Seki, K., Study of the interaction of tris-(8-hydroxyquinoline) aluminum (Alq_3) with potassium using vibrational spectroscopy: Examination of possible isomerization upon K doping, *J. Appl. Phys.*, Vol. 96, No. 10 (2004), pp. 5534-5542.

Salaneck, W. R.; Seki, K.; Kahn, A.; Pireaux, J. J., (Eds.) 2002, *Conjugated Polymer and Molecular Interfaces – Science and Technology for Photonic and Optoelectronics Applications*, Marcel Dekker, ISBN 0-8247-0588-2, New York.

Seki, K.; Ito, E.; Ishii, H., Energy level alignment at organic/metal interfaces studied by UV photoemission, *Synth. Met.,* Vol. 91, Nos. 1-3 (1997), pp. 137-142.

Shaheen, S. E.; Jabbour, G. E.; Morrell, M. M.; Kawabe, Y.; Kippelen, B.; Peyghambarian, N.; Nabor, M. –F.; Schlaf, R.; Mash, E. A.; Armstrong, N. R., Bright blue organic light-emitting diode with improved color purity using a LiF/Al cathode, *J. Appl. Phys.*, Vol. 84, No. 4 (1998), pp. 2324-2327.

Shen, Y. R., November 2002, *The principles of Nonlinear Optics*: Wiley, ISBN: 978-0-471-43080-3, New York.

Silva, H. S.; Miranda, P. B., Molecular ordering of layer-by-layer polyelectrolyte films studied by sum-frequency vibrational spectroscopy, *J. Phys. Chem. B*, Vol. 113, No. 30 (**2009)**, pp. 10068–10071.

Sugi, K.; Ishii, H.; Kimura, Y.; Niwano, M.; Ito, E.; Washizu, Y.; Hayashi, N.; Ouchi, Y.; Seki, K., Characterization of light-erasable giant surface potential built up in evaporated Alq_3 thin films, *Thin Solid Films*, Vol. 464-465 (2004), pp. 412-415.

Tang, C. W.; Slyke, S. A. V, Organic electroluminescent diodes, *Appl. Phys. Lett.*, Vol. 51, No. 12 (1987), pp. 913-915.

Wei, X.; Hong, S. C.; Lvovsky, A. I.; Held, H.; Shen, Y. R., Evaluation of surface vs bulk contributions in sum-frequency vibrational spectroscopy using reflection and transmission geometries, *J. Phys. Chem. B*, Vol. 104, No. 14 (2000), pp. 3349-3354.

Wu, D.; Deng, G. H.; Guo, Y.; Wang, H. F., Observation of the interference between the intramolecular IR−visible and visible−IR processes in the doubly resonant sum frequency generation vibrational spectroscopy of rhodamine 6G adsorbed at the air/water interface, *J. Phys. Chem. A*, Vol. 113, No. 21 (2009), pp. 6058-6063.

Yanagisawa, S; Morikawa, Y., Theoretical investigation on the electronic structure of the tris-(8-hydroxyquinolinato) aluminum/aluminum interface, *Jpn. J. Appl. Phys.,* Vol. 45, No. 1B (2006), pp. 413-416.

Yanagisawa, S.; Lee, K.; Morikawa, Y., First-principles theoretical study of Alq_3/Al interfaces: Origin of the interfacial dipole, *J. Chem. Phys.*, Vol. 128, No. 24 (2008), pp. 244704.

Yokoyama, T.; Yoshimura, D.; Ito, E.; Ishii, H.; Ouchi, Y.; Seki, K., Energy level alignment at Alq_3/LiF/Al interfaces studied by electron spectroscopies: Island growth of LiF and size-dependence of the electronic structures, *Jpn. J. Appl. Phys.*, Vol. 42, No. 6A, (2003), pp. 3666-3675.

Yokoyama, T.; Ishii, H.; Matsuie, N.; Kanai, K.; Ito, E.; Fujimori, A.; Araki, T.; Ouchi, Y.; Seki, K., Neat Alq_3 thin film and metal/Alq_3 interfaces studied by NEXAFS spectroscopy, *Synth. Met.* Vol. 152, No. 1-3, (2005), pp. 277-280.

Yoshizaki, K.; Manaka, T.; Iwamoto, M., Large surface potential of Alq_3 film and its decay, *J. Appl. Phys.*, Vol. 97, No. 2, (2005), pp. 023703.

Zhu, R.; Lin, J. M.; Wang, W. Z.; Zheng, C.; Wei, W.; Huang, W.; Xu, Y. H.; Peng, J. B.; Cao,Y., Use of the β-phase of poly(9,9-dioctylfluorene) as a probe into the interfacial interplay for the mixed bilayer films formed by sequential spin-coating, *J. Phys. Chem. B*, Vol. 112, No. 6 (2008), pp. 1611-1618.

Zhuang, X.; Miranda, P. B.; Kim, D.; Shen, Y. R., Mapping molecular orientation and conformation at interfaces by surface nonlinear optics, *Phys. Rev. B*, Vol. 59, No. 19 (1999), pp. 12632-12640.

IntechOpen

IntechOpen

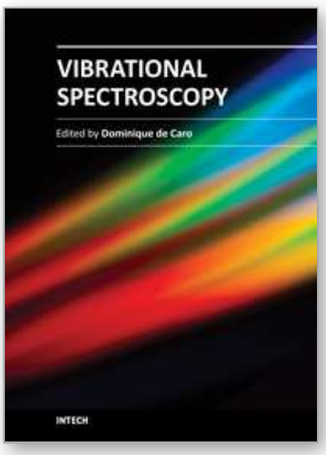

Vibrational Spectroscopy
Edited by Prof. Dominique De Caro

ISBN 978-953-51-0107-9
Hard cover, 168 pages
Publisher InTech
Published online 24, February, 2012
Published in print edition February, 2012

The infrared and Raman spectroscopy have applications in numerous fields, namely chemistry, physics, astronomy, biology, medicine, geology, mineralogy etc. This book provides some examples of the use of vibrational spectroscopy in supramolecular chemistry, inorganic chemistry, solid state physics, but also in the fields of molecule-based materials or organic-inorganic interfaces.

How to reference
In order to correctly reference this scholarly work, feel free to copy and paste the following:

Takayuki Miyamae (2012). Probing Metal/Organic Interfaces Using Doubly-Resonant Sum Frequency Generation Vibrational Spectroscopy, Vibrational Spectroscopy, Prof. Dominique De Caro (Ed.), ISBN: 978-953-51-0107-9, InTech, Available from: http://www.intechopen.com/books/vibrational-spectroscopy/probing-metal-organic-interfaces-using-doubly-resonant-sum-frequency-generation-spectroscopy

INTECH
open science | open minds

InTech Europe
University Campus STeP Ri
Slavka Krautzeka 83/A
51000 Rijeka, Croatia
Phone: +385 (51) 770 447
Fax: +385 (51) 686 166
www.intechopen.com

InTech China
Unit 405, Office Block, Hotel Equatorial Shanghai
No.65, Yan An Road (West), Shanghai, 200040, China
中国上海市延安西路65号上海国际贵都大饭店办公楼405单元
Phone: +86-21-62489820
Fax: +86-21-62489821

© 2012 The Author(s). Licensee IntechOpen. This is an open access article distributed under the terms of the Creative Commons Attribution 3.0 License, which permits unrestricted use, distribution, and reproduction in any medium, provided the original work is properly cited.

IntechOpen

IntechOpen